PHYSICAL REVIEW B **89**, 220503(R) (2014)

Coexistence of orbital degeneracy lifting and superconductivity in iron-based superconductors

H. Miao,[1] L.-M. Wang,[2] P. Richard,[1,3,*] S.-F. Wu,[1] J. Ma,[1] T. Qian,[1] L.-Y. Xing,[1] X.-C. Wang,[1] C.-Q. Jin,[1,3] C.-P. Chou,[2,4] Z. Wang,[5] W. Ku,[2] and H. Ding[1,3,†]

[1]*Beijing National Laboratory for Condensed Matter Physics, and Institute of Physics, Chinese Academy of Sciences, Beijing 100190, China*
[2]*Condensed Matter Physics and Materials Science Department, Brookhaven National Laboratory, Upton, New York 11973, USA*
[3]*Collaborative Innovation Center of Quantum Matter, Beijing, China*
[4]*Beijing Computational Science Research Center, Beijing 100084, China*
[5]*Department of Physics, Boston College, Chestnut Hill, Massachusetts 02467, USA*

(Received 29 January 2014; revised manuscript received 29 May 2014; published 11 June 2014)

We report the angle-resolved photoemission spectroscopy observation of the lifting of symmetry-protected band degeneracy, and consequently the breakdown of local tetragonal symmetry in the superconducting state of Li($Fe_{1-x}Co_x$)As. Supported by theoretical simulations, we analyze the doping and temperature dependences of this band splitting and demonstrate an intimate connection between ferro-orbital correlations and superconductivity.

DOI: 10.1103/PhysRevB.89.220503 PACS number(s): 74.25.Jb, 74.20.Mn, 74.70.Xa, 79.60.−i

In contrast to conventional superconducting (SC) materials, superconductivity in high-temperature superconductors (HTSCs) usually emerges in the presence of other fluctuating orders with similar or higher-energy scales [1–4], thus instigating debates over their relevance for the SC pairing mechanism. Although spin fluctuations are widely believed to be crucial for unconventional superconductivity, orbital fluctuations in the multiorbital iron-based superconductors (IBSCs) are proposed to be directly responsible for the structural phase transition [5,6] and closely related to the observed giant magnetic anisotropy and electronic nematicity [7–13]. More recently, fluctuating orbital order has been proposed to lead to an attractive mechanism for pairing [14,15] and further raised the following question: Can superconductivity coexist with or even emerge from orbital fluctuations?

In the tetragonal phase without spin-orbital coupling (SOC), the d_{xz}/d_{yz} orbitals are degenerate at the Brillouin zone center (Γ point), which is guaranteed by point-group symmetry. Ferro-orbital (FO) order, which leads to unequal occupation of the d_{xz}/d_{yz} orbitals, would lift the degeneracy at Γ, resulting in a band gap Δ_{band} that can be monitored directly by angle-resolved photoemission spectroscopy (ARPES). While FO fluctuations have been proposed as the origin of electronic nematicity [5,6] and can be closely related to the emergence of superconductivity [14,15], probing FO fluctuations directly in the absence of structural and magnetic phase transitions needs to be explored, and whether FO fluctuations coexist or compete with the SC order is still an open question.

In this Rapid Communication, we report the ARPES observation of the lifting of symmetry-protected band degeneracy, and consequently the breakdown of local tetragonal symmetry in the SC state of Li($Fe_{1-x}Co_x$)As. By analyzing the doping and temperature dependences of this band splitting and using theoretical simulations, we demonstrate that the splitting is caused by power-law decayed ferro-orbital correlations and prove its intimate connection with superconductivity.

Single crystals of $LiFe_{1-x}Co_xAs$ were synthesized by a self-flux method using Li_3As, $Fe_{1-x}Co_xAs$, and As powders as the starting materials. The mixture was grounded and put into alumina crucible and sealed in Nb crucibles under 1 atm of argon gas. The Nb crucible was then sealed in an evacuated quartz tube, heated to 1100 °C, and slowly cooled down to 700 °C at a rate of 3 °C/h. High-energy resolution ARPES data were recorded at the Institute of Physics, Chinese Academy of Sciences, using the He Iα ($h\nu = 21.2$ eV) resonance line of an helium discharge lamp. The angular and momentum resolutions were set to 0.2° and 3 meV, respectively. ARPES polarization measurements were performed at beamlines PGM and Apple-PGM of the Synchrotron Radiation Center (Wisconsin) equipped with a Scienta R4000 analyzer and a Scienta SES 200 analyzer, respectively. The energy and angular resolutions were set at 20 meV and 0.2°, respectively. All samples were cleaved *in situ* and measured in a vacuum better than 3×10^{-11} Torr.

In addition to having a natural nonpolar cleaving surface preserving its bulk properties [16–18], Li($Fe_{1-x}Co_x$)As has neither structural nor magnetic phase transitions in its whole phase diagram [19], enabling us to study fluctuations in the absence of long-range orders. In Fig. 1, we compare the electronic band dispersion of LiFeAs and $LiFe_{0.88}Co_{0.12}As$ at 20 K around the Γ point. Our polarization analysis confirms that the α and α′ bands, which are mainly composed of d_{xz}/d_{yz} orbitals, have odd and even symmetries, respectively [20–22]. The extracted band dispersion [23] in $LiFe_{0.88}Co_{0.12}As$ ($T_c = 4$ K) indicates that both the α and α′ bands sink below E_F and are exactly degenerate at the Γ point, as required by symmetry. In contrast, the α band crosses E_F at $k_F = 0.03\pi/a$ in the parent compound LiFeAs ($T_c = 18$ K), whereas the top of the α band lies about 12 meV below E_F, which means that the d_{xz}/d_{yz} orbitals are split in LiFeAs without long-range magnetic and orbital orders. To precisely resolve the band splitting, we recorded very-high-energy resolution ARPES intensity plots of LiFeAs and $LiFe_{0.88}Co_{0.12}As$, as shown in Fig. 1. From the high-resolution data, we evaluate the band gap to $\Delta_{\text{band}} \sim 14$ meV in LiFeAs by extrapolating the top of the α band using a parabolic fit, and we confirm the degeneracy of the d_{xz}/d_{yz} bands in

*p.richard@iphy.ac.cn
†dingh@iphy.ac.cn

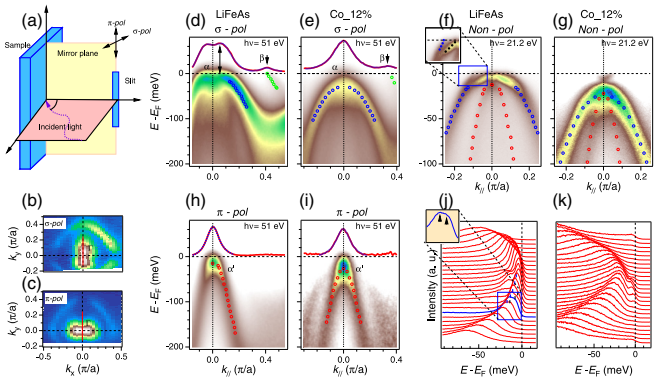

FIG. 1. (Color online) (a) ARPES experimental geometry. (b), (c) FS mapping at the Brillouin zone center measured under σ and π configurations. (d), (h) ARPES intensity plots of LiFeAs measured along the Γ-M direction [the red line in (b) and (c)], and recorded with 51 eV incident light in the σ and π configurations to select odd and even orbital symmetries [20–22], respectively. (e), (i) Same as (d) and (h), but for $LiFe_{0.88}Co_{0.12}As$. (f), (g) High-energy resolution ARPES cuts along the Γ-M direction of LiFeAs and $LiFe_{0.88}Co_{0.12}As$, respectively, recorded with the He Iα line of an helium discharge lamp. The red and blue curves in (d), (e), (h), and (i) are the original and fitted momentum distribution curves at E_F, respectively. The blue, red, and green circles represent the peak positions associated with the α (d_{odd}), α' (d_{even}), and β (d_{xy}) bands, respectively, where d_{odd} (d_{even}) is the odd (even) linear combination of the d_{xz} and d_{yz} orbitals. (j), (k) EDCs corresponding to the data shown in (f) and (g), respectively. The blue EDC in (j), also shown in inset, illustrates the splitting of the α band.

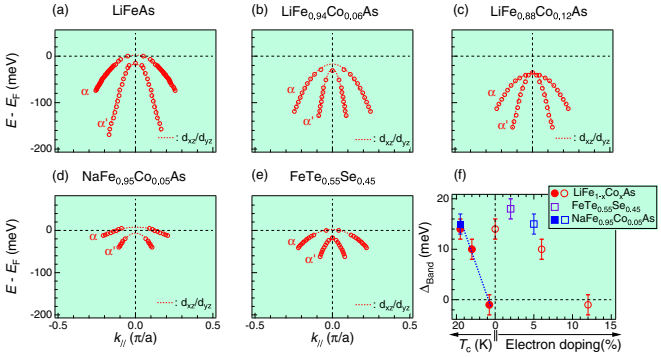

FIG. 2. (Color online) (a)–(c) Extracted band dispersion of the d_{xz}/d_{yz} bands in LiFeAs, $LiFe_{0.94}Co_{0.06}As$ [22], and $LiFe_{0.88}Co_{0.12}As$, respectively. (d), (e) Extracted band dispersion of $NaFe_{0.95}Co_{0.05}As$ [26] and $FeTe_{0.55}Se_{0.45}$ [27], respectively. Red dashed curves are parabolic fits. (f) Doping and T_c dependence of Δ_{band}. The open and solid symbols refer to the doping (bottom right) and T_c (bottom left) axes. Error bars are determined by standard deviation of the fitting parameters [22].

$LiFe_{0.88}Co_{0.12}As$. By zooming near E_F, we find that the α band further splits into two branches, as shown in Figs. 1(f) and 1(j). While one branch is the continuous extension of the high binding energy dispersion, the other one shows an inflection point at 14 meV binding energy. A similar effect is also observed on the electron band [22] and, as discussed later, the observed fine structure is caused by twin domains and supports that the observed band splitting is caused by FO fluctuations. As reported previously [24], we distinguish an electron band at the Γ point of electron-doped $LiFe_{0.88}Co_{0.12}As$, which is not clear in the synchrotron-based results, most likely due to different k_z positions. We suspect that this small electron band has a strong As p_z orbital component and is similar to the one observed in $(Tl,Rb)_yFe_{2-x}Se_2$ [25].

To check whether the d_{xz}/d_{yz} splitting is a general feature of the IBSCs, we performed similar experiments on various materials and summarized the results in Fig. 2. We first considered $LiFe_{0.94}Co_{0.06}As$ ($T_c = 10$ K), which has an intermediate doping between LiFeAs and $LiFe_{0.88}Co_{0.12}As$ [22]. Unlike in LiFeAs and similarly to $LiFe_{0.88}Co_{0.12}As$, the α band falls below E_F. For this material, we find $\Delta_{\text{band}} = 10$ meV, suggesting that the band splitting is gradually suppressed as T_c decreases from 18 to 4 K. We also studied the band splitting in $NaFe_{0.95}Co_{0.05}As$ ($T_c = 18$ K) [26], which is isostructural to LiFeAs (the so-called 111 structure). From the extracted band dispersions displayed in Fig. 2(d), we deduce that $\Delta_{\text{band}} = 15$ meV in this particular compound. Interestingly, as shown in Fig. 2(f), all our data on the 111 crystal structure indicate that Δ_{band} scales with T_c in this family of materials, suggesting that the band splitting might be related to superconductivity. Interestingly, there is at least one other IBSC for which a d_{xz}/d_{yz} band splitting is clearly observed. Indeed, this observation has been reported for the $FeTe_{1-x}Se_x$ family of IBSCs [27,28]. Using the data from Miao *et al.* [27], reproduced in Fig. 2(e), we find that $\Delta_{\text{band}} = 18$ meV in $FeTe_{0.55}Se_{0.45}$, which is even larger than in LiFeAs. The observed band splitting in all the IBSCs studied here strongly suggests that the d_{xz}/d_{yz} separation at the Γ point has a fundamental origin.

We now focus on the temperature evolution of Δ_{band} in LiFeAs. For this purpose, we show in Fig. 3 high-energy resolution ARPES cuts across the Γ point recorded between 50 and 250 K. The data are divided by the Fermi-Dirac function convoluted by the resolution function to reveal the band dispersion above E_F, which are obtained from parabolic fits. While the linewidths of the α' and β bands broaden with temperature, their dispersions are unaffected. The α band, on the other hand, gradually shifts downward and its top almost merges with that of the α' band at 250 K. In Fig. 3(m), we show the evolution of Δ_{band} as a function of temperature by using different methods that all show that the d_{xz}/d_{yz} splitting decreases gradually from nearly 0 at 250 K to about 14 meV at 50 K [22]. Interestingly, the splitting survives even below the SC phase transition at 18 K. As shown in Figs. 3(n)–3(p), the α band opens up a SC gap below T_c, whereas the α' band is barely changed. This observation proves that the band splitting coexists with superconductivity.

The observed degeneracy lifting by ARPES at the Γ point reflects directly the difference in site energy of the d_{xz} and d_{yz} orbitals at low energies, which is a direct measurement of the ferro-orbital configuration, regardless of the origin of the mechanism driving the system into this configuration. In order to demonstrate that FO fluctuations can lead to the removal of a symmetry-imposed degeneracy, even in the absence of long-range ordering, we investigate a simple model of a quasi-one-dimensional (1D) electronic system (since d_{xz}/d_{yz} orbitals have strongly anisotropic quasi-1D hopping integrals) under the influence of a spatially fluctuating local FO order parameter (represented by a diagonal Ising field) [21,22], and

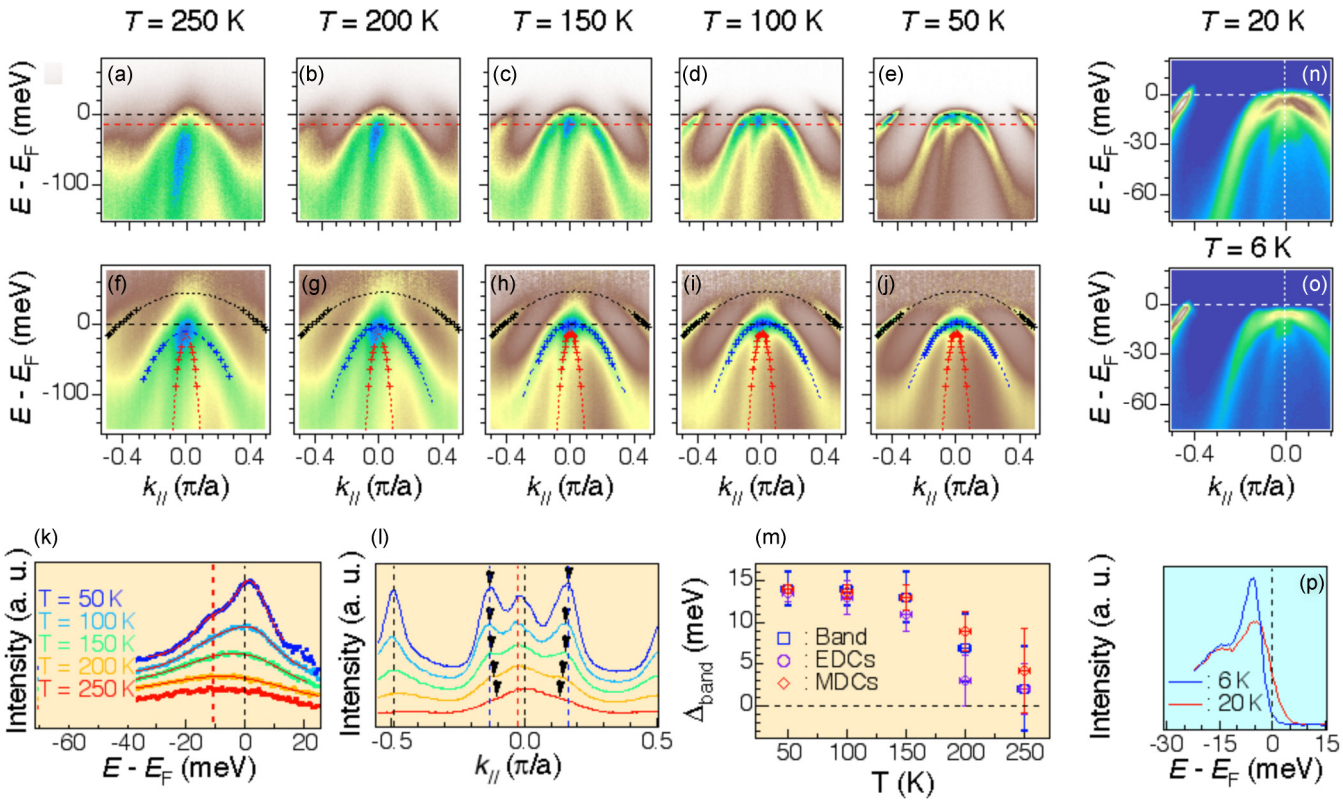

FIG. 3. (Color online) (a)–(e) High-energy resolution ARPES intensity plots at $T = 250$, 200, 150, 100, and 50 K, respectively. (f)–(j) Same data but divided by the Fermi-Dirac function convoluted with the system resolution function to probe the electronic structure above E_F. Band dispersions at different temperatures are extracted using momentum distribution curves (MDCs) and fitted to parabolic functions. (k) Energy distribution curves (EDCs) at the Γ point at different temperatures. We used two Lorentzian peaks to extract the top of the α and α' bands, and plot the fitted results on top of the original data using red dashed curves [22]. The top of the α band is shifted towards high binding energy as temperature increases, and it almost merges with the top of the α' band at 250 K. (l) MDCs recorded 20 meV below E_F, which corresponds to the red dashed lines shown in (a)–(e). At high temperature, the α peak positions move towards Γ, indicating that the band moves downward in energy. In contrast, the peak positions of the α' and β bands are unchanged [22]. (m) Temperature evolution of Δ_{band}. The values of Δ_{band} are extracted from the electronic band dispersions, EDCs and MDCs. Error bars are determined by the standard deviation of the fitted parameters. (n) and (o) are ARPES intensity plots just above and well below T_c, respectively. (p) EDCs at the Γ point above and below T_c.

we display the results in Fig. 4. When the local order parameter has only short-range correlations (exponential decay), no clear indication of the fluctuating order is observed in the electronic structure other than the scattering of the particle that broadens the spectral function, as illustrated in the top row of Fig. 4. In contrast, when the spatial correlations of the local order parameter are long ranged (power-law decay), the quasiparticle peak splits in two and a pseudogap in the spectral function develops in between, as shown in Figs. 4(f)–4(h). This pseudogap corresponds to the splitting of the degenerate bands shown in Fig. 1. Although the spectral function exhibits features identical to those expected in the presence of a macroscopic long-range order, we emphasize that the system has not yet developed a true order, but only long-range spatial correlations. In other words, the one-particle Green's function has gone ahead and reflects the underlying, almost ordered, electronic structure. Therefore, the experimentally observed doping-dependent splitting between the d_{xz}/d_{yz} bands in the absence of FO order can be attributed to strong, slow-decaying, long-range FO correlations that cover a large region of the phase diagram and eventually support superconductivity at low temperature. We stress that although our minimal two-orbital model indicates that a fluctuating diagonal order parameter is capable of lifting a degeneracy required by symmetry, one should be cautious when comparing our models with realistic band structures. In real systems, the self-energy induced by the fluctuating ferro-orbital order parameter should be momentum, energy and orbital dependent, and thus exhibit rich variations.

Very recently, an electronic Raman scattering study of $Ba(Fe_{1-x}Co_x)_2As_2$ [29], an ARPES study [9], and a combined study of magnetic torque and x ray in $BaFe_2(As_{1-x}P_x)_2$ [13] reported electronic nematicity in the absence of a magnetic phase transition. The observed nematic signal persists far above the SC and structural phase transitions, indicating the presence of a strong fluctuating orbital order, which is consistent with our doping- and temperature-dependent results, as well as with our theoretical interpretation. However, alternative mechanisms could also lead indirectly to the lifting of the band degeneracy. For example, although the *C*-type (collinear) antiferromagnetic (AF) correlations do not directly contribute to the observed band degeneracy lifting, they could do so when coupled to the orbital degree of freedom, as predicted by theoretical studies [5,6,30,31]. Nevertheless, in the present study, we find that superconductivity emerges

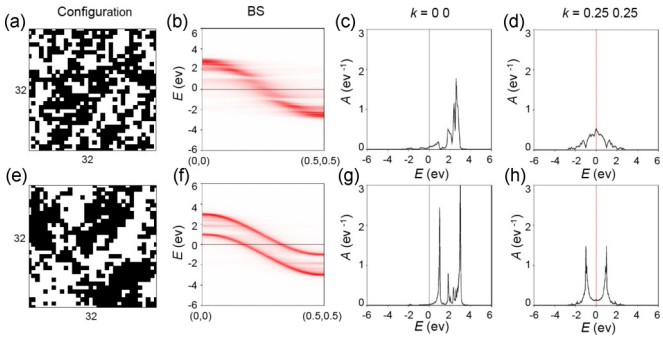

FIG. 4. (Color online) (a) An example of the configuration of a FO disordered system (represented by an Ising field) without long-range correlations. (b) The resulting average band structure that couples to the Ising field, showing no clear splitting of the band. (c), (d) The average spectral function at momentum $k = (0,0)$ and $k = (0.25,0.25)$. (e)–(h) Similar to (a)–(d), however, the disordered system contains long-range, power-law decaying correlations of the local order parameter.

in the regime of strong FO correlations and that the SC transition temperature scales with the strength of the local orbital order, suggesting an intimate connection between FO correlations and superconductivity. This observation is very important since a recent ARPES and NMR study reports enhancement of low-energy antiferromagnetic spin fluctuations in $LiFe_{1-x}Co_xAs$ samples with lower T_c [24], thus suggesting that such low-energy antiferromagnetic fluctuations alone do not control the strength of superconductivity in $LiFe_{1-x}Co_xAs$.

Finally, we discuss the effect of SOC. In principle, SOC can lift the degeneracy of the d_{xz}/d_{yz} orbitals at the Γ point while maintaining global tetragonal symmetry [32]. However, since SOC is a local effect and barely changes with doping and temperature, our observation of Δ_{band} variations as a function of doping and temperature is inconsistent with this scenario. Moreover, we carefully extracted the electronic band structure near the M point and found that the degeneracy between d_{xz} and d_{yz} at the M point is lifted with a splitting gap $\Delta_M = 8$ meV, which is smaller than the splitting at the Γ point [22]. All the experimental facts support our assumption that the observed d_{xz}/d_{yz} splitting at the Γ point is caused by FO fluctuations instead of SOC. Although spin fluctuations have been widely studied and discussed, few experimental studies on the orbital fluctuations can be found in the literature. Our study provides evidence for strong, long-range FO correlations in IBSCs and demonstrates their intimate connection with superconductivity in $LiFe_{1-x}Co_xAs$.

We thank A. Tsvelik, J.-P. Hu, F. Wang, P. D. Johnson, and H.-B. Yang for useful discussions. This work was supported by grants from CAS (No. 2010Y1JB6), MOST (No. 2010CB923000, No. 2011CBA001000, and No. 2013CB921703), and NSFC (No. 11004232 and No. 11274362). The theoretical study is supported by U.S. Department of Energy, Office of Science DE-AC02-98CH10886. This work is based in part on research conducted at the Synchrotron Radiation Center, which is primarily funded by the University of Wisconsin-Madison with the University of Wisconsin-Milwaukee.

[1] D. Aoki, A. Huxley, E. Ressouche, D. Braithwaite, J. Flouquet, J. Brison, E. Lhotel, and C. Paulsen, Nature (London) **413**, 613 (2001).
[2] J. M. Tranquada, H. Woo, T. G. Perring, H. Goka, G. D. Gu, G. Xu, M. Fujita, and K. Yamada, Nature (London) **429**, 534 (2004).
[3] J. M. Tranquada, J. D. Axe, N. Ichikawa, A. R. Moodenbaugh, Y. Nakamura, and S. Uchida, Phys. Rev. Lett. **78**, 338 (1997).
[4] D. K. Pratt, W. Tian, A. Kreyssig, J. L. Zarestky, S. Nandi, N. Ni, S. L. Bud'ko, P. C. Canfield, A. I. Goldman, and R. J. McQueeney, Phys. Rev. Lett. **103**, 087001 (2009).
[5] C.-C. Lee, W.-G. Yin, and W. Ku, Phys. Rev. Lett. **103**, 267001 (2009).
[6] W.-C. Lv, F. Krüger, and P. Phillips, Phys. Rev. B **82**, 045125 (2010).
[7] T.-M. Chuang, M. P. Allan, J. Lee, Y. Xie, N. Ni, S. L. Bud'ko, G. S. Boebinger, P. C. Canfield, and J. C. Davis, Science **327**, 181 (2010).
[8] J.-H. Chu, J. G. Analytis, K. D. Greve, P. L. McMahon, Z. Islam, Y. Yamamoto, and I. R. Fisher, Science **329**, 824 (2010).
[9] T. Shimojima *et al.*, Phys. Rev. B **89**, 045101 (2014).
[10] M. Yi, D.-H. Lu, J.-H. Chu, J. G. Analytis, A. P. Sorini, A. F. Kemper, B. Moritz, S. K. Mo, R. G. Moore, M. Hashimoto, W.-S. Lee, Z. Hussain, T. P. Devereaux, I. R. Fisher, and Z.-X. Shen, Proc. Natl. Acad. Sci. USA **108**, 6878 (2011).
[11] M. Yi, D. H. Lu, R. G. Moore, K. Kihou, C.-H. Lee, A. Iyo, H. Eisaki, T. Yoshida, A. Fujimori, and Z. X. Shen, New J. Phys. **14**, 073019 (2012).
[12] H.-H. Hung, C. L. Song, X. Chen, X. Ma, Q. K. Xue, and C. Wu, Phys. Rev. B **85**, 104510 (2012).
[13] S. Kasahara, H. J. Shi, K. Hashimato, S. Tonegawa, Y. Mizukami, T. Shibauchi, K. Sugimoto, T. Fukuda, T. Terashima, A. H. Nevidomskyy, and Y. Matsuda, Nature (London) **486**, 382 (2012).
[14] H. Kontani and S. Onari, Phys. Rev. Lett. **104**, 157001 (2010).
[15] S. Zhou, G. Kotliar, and Z. Wang, Phys. Rev. B **84**, 140505 (2011).
[16] K. Umezawa, Y. Li, H. Miao, K. Nakayama, Z.-H. Liu, P. Richard, T. Sato, J. B. He, D.-M. Wang, G. F. Chen, H. Ding, T. Takahashi, and S.-C. Wang, Phys. Rev. Lett. **108**, 037002 (2012).
[17] S. V. Borisenko, V. B. Zabolotnyy, D. V. Evtushinsky, T. K. Kim, I. V. Morozov, A. N. Yaresko, A. A. Kordyuk, G. Behr, A. Vasiliev, R. Follath, and B. Büchner, Phys. Rev. Lett. **105**, 067002 (2010).
[18] M. P. Allan, A. W. Rost, A. P. Mackenzie, Y. Xie, J. C. Davis, K. Kihou, C. H. Lee, A. Iyo, H. Eisaki, and T.-M. Chuang, Science **336**, 563 (2012).
[19] X.-C. Wang, Q. Q. Liu, Y. X. Lv, W. B. Gao, L. X. Yang, R. C. Yu, F. Y. Li, and C. Q. Jin, Solid State Commun. **148**, 538 (2008).

[20] X.-P. Wang, P. Richard, Y.-B. Huang, H. Miao, L. Cevey, N. Xu, Y.-J. Sun, T. Qian, Y.-M. Xu, M. Shi, J.-P. Hu, X. Dai, and H. Ding, Phys. Rev. B **85**, 214518 (2012).

[21] C.-H. Lin, T. Berlijn, L.-M. Wang, C.-C. Lee, W.-G. Yin, and W. Ku, Phys. Rev. Lett. **107**, 257001 (2011).

[22] See Supplemental Material at http://link.aps.org/supplemental/10.1103/PhysRevB.89.220503 for additional details of data analysis and theoretical support.

[23] P. D. Johnson, T. Valla, A. V. Fedorov, Z. Yusof, B. O. Wells, Q. Li, A. R. Moodenbaugh, G. D. Gu, N. Koshizuka, C. Kendziora, S. Jian, and D. G. Hinks, Phys. Rev. Lett. **87**, 177007 (2001).

[24] Z.-Y. Ye, M. Xu, Q. Q. Ge, Q. Fan, F. Chen, J. Jiang, P. S. Wang, J. Dai, W. Yu, B. P. Xie, and D. L. Feng, arXiv:1303.0682.

[25] Z.-H. Liu, P. Richard, N. Xu, G. Xu, Y. Li, X.-C. Fang, L.-L. Jia, G.-F. Chen, D.-M. Wang, J.-B. He, T. Qian, J.-P. Hu, H. Ding, and S.-C. Wang, Phys. Rev. Lett. **109**, 037003 (2012).

[26] Z.-H. Liu, P. Richard, K. Nakayama, G.-F. Chen, S. Dong, J.-B. He, D.-M. Wang, T.-L. Xia, K. Umezawa, T. Kawahara, S. Souma, T. Sato, T. Takahashi, T. Qian, Y.-B. Huang, N. Xu, Y.-B. Shi, H. Ding, and S.-C. Wang, Phys. Rev. B **84**, 064519 (2011).

[27] H. Miao, P. Richard, Y. Tanaka, K. Nakayama, T. Qian, K. Umezawa, T. Sato, Y.-M. Xu, Y.-B. Shi, N. Xu, X.-P. Wang, P. Zhang, H.-B. Huang, Z.-J. Xu, J. S. Wen, G.-D. Gu, X. Dai, J.-P. Hu, T. Takahashi, and H. Ding, Phys. Rev. B **85**, 094506 (2012).

[28] S.-Y. Tan, Y. Zhang, M. Xia, Z. R. Ye, F. Chen, X. Xie, R. Peng, D. F. Xu, Q. Fan, H. C. Xu, J. Jiang, T. Zhang, X. C. Lai, T. Xiang, J. P. Hu, B. P. Xie, and D. L. Feng, Nat. Mater. **12**, 634 (2013).

[29] Y. Gallais, R. M. Fernandes, I. Paul, L. Chauviere, Y. X. Yang, M.-A. Measson, M. Cazayous, A. Sacuto, D. Colson, and A. Forget, Phys. Rev. Lett. **111**, 267001 (2013).

[30] M. Daghofer, Q.-L. Luo, R. Yu, D. X. Yao, A. Moreo, and E. Dagotto, Phys. Rev. B **81**, 180514 (2010).

[31] R. M. Fernandes, A. V. Chubokov, J. Knolle, I. Eremin, and J. Schmalian, Phys. Rev. B **85**, 024534 (2012).

[32] V. Cvetkovic and O. Vafek, Phys. Rev. B **88**, 134510 (2013).

Supplementary Materials for

Coexistence of orbital degeneracy lifting and superconductivity in iron-based superconductors

H. Miao[1], L. -M. Wang[2], P. Richard[1,3*], S. –F. Wu[1], J. Ma[1], T. Qian[1], L. -Y. Xing[1], X. -C. Wang[1], C. -Q. Jin[1,3], C. -P. Chou[4,2], Z. Wang[5], W. Ku[2], and H. Ding[1,3‡]

To whom correspondence should be addressed.

*: p.richard@aphy.iphy.ac.cn;

‡: dingh@aphy.iphy.ac.cn

This PDF file includes:

Table of contents

1. Single crystals:

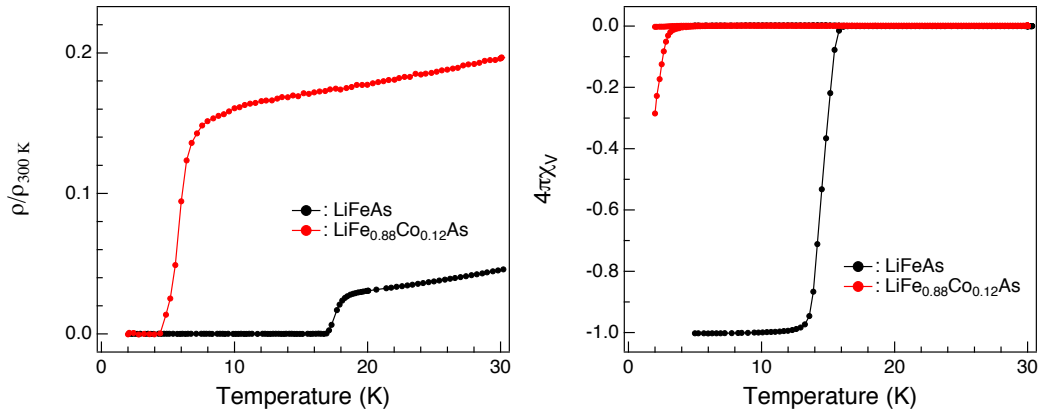

S1: Resistivity and magnetic susceptibility of $LiFe_{1-x}Co_xAs$

Fig. S1 shows transport properties of the samples we used to perform ARPES experiments. The high quality of the samples is characterized by the narrow superconducting transition temperature and high superconducting volume.

2. ARPES:

2.1 ARPES matrix element effect and experimental geometry.

The process of photoemission is usually described by the so-called three-step model[1]: electrons are excited from their initial states |i>, they then travel

towards the surface and finally reach their final states $|f\rangle$. In this simplified model, the ARPES matrix element is formulated as:

$$M_{ij} = \langle f | A \bullet r | i \rangle \qquad (1)$$

Where **A** is the potential vector associated with the incoming photon and **r** is position operator. Since $|M_{ij}|^2$ is a scalar observable, it does not change under the symmetry operations of the relevant crystal structure, which is possible only if its total parity is even (+). Simple rules can thus be used to know whether the photoemission matrix element can be non-zero. Since the final state $\langle f|r\rangle$ is approximately a plane wave and has even symmetry, the total parity of M_{ij} will be decided by combinations of A•r and the initial state, as shown in Eq. (2):

$$\begin{array}{l} \langle + | + | + \rangle \neq 0, \langle + | + | - \rangle = 0 \\ \langle + | - | - \rangle \neq 0, \langle + | - | + \rangle = 0 \end{array} \qquad (2)$$

The experimental setup used in this study is shown in Fig. S2, where the π- and σ- polarizations are defined as the incident potential vector being parallel and perpendicular to the mirror plane, respectively. According to Eq. (2), π-polarization and σ-polarization select the even and odd orbital symmetry of the initial state, respectively.

.

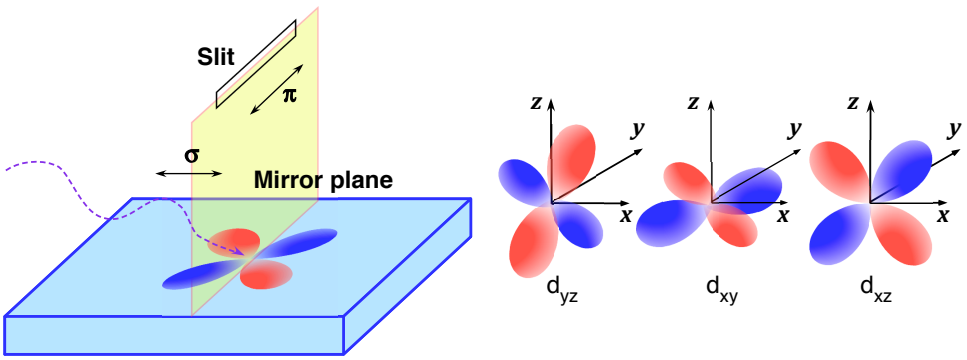

S2: Experimental geometry

2.2 The k_z effect

In Figs. S3a and 3b we show ARPES intensity plots of LiFeAs recorded with 35 eV incident light, which corresponds to $k_z = \pi$, in the σ and π configurations, respectively. By extracting the dispersion of the α and α' bands from MDCs, we are able to estimate the variation of the band splitting along k_z. As shown in Fig. S3c, the α band (d_{odd}) is very two-dimensional while the α' band (d_{even}) has a k_z dispersion, which is consistent with other iron-based superconductors. Due to the k_z dispersion of the α' band, the band splitting is increased to 34 meV at $k_z = \pi$. The band splitting along k_z can be estimated by:

$$\Delta_{band}=24-10\cos(k_z) \qquad (3)$$

In the free-electron final-state approximation, the value of k_z can be calculated by:

$$k_z = \frac{c}{2\pi\hbar}\sqrt{(\hbar\nu - \phi - E_B)\cos^2\theta + V_0} \quad (4)$$

Where V_0 is an experimentally determined inner potential[2]. In $LiFe_{1-x}Co_xAs$, V_0 is determined to be 14 eV, which is very similar to $Ba_{1-x}K_xFe_2As_2$[2].

When Co is doped into LiFeAs, the *c*-lattice parameter is changed from 6.36372 Å in LiFeAs to 6.32262 Å in $LiFe_{0.88}Co_{0.12}As$. According to Eqs. (3) and (4) and considering the k_z average effect of ARPES[3] we conclude that:

$$\delta\Delta_{band} \sim 1 \text{ meV}$$

which is smaller than the error bar.

Therefore, we can safely draw the conclusion that the k_z effect can be neglected in Fig. 2f of the main text.

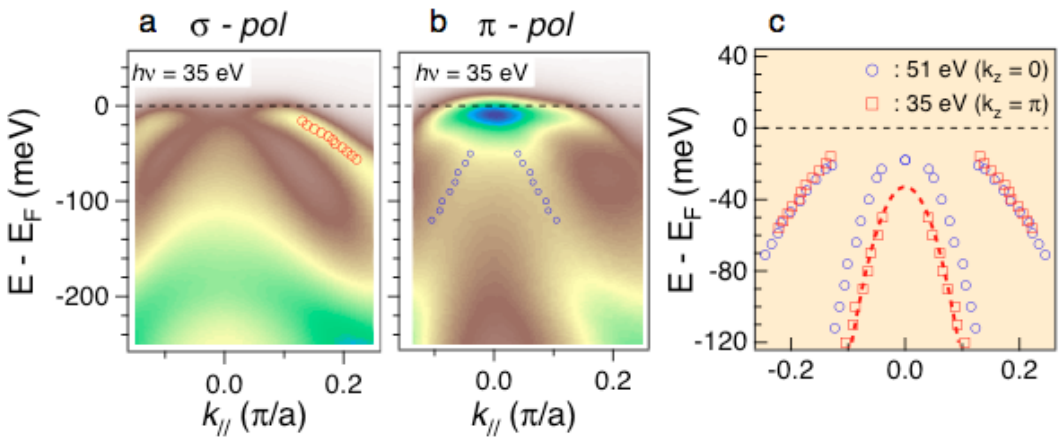

S3: ARPES intensity plot at $k_z = \pi$

2.3 $LiFe_{0.94}Co_{0.06}As$

Fig. S4 shows an ARPES intensity plot and EDCs of $LiFe_{0.94}Co_{0.06}As$. The band dispersions of the α, α' and β bands are carefully extracted from EDCs and MDCs and fitted to a parabolic function. The band splitting is clearly resolved from both the intensity plot and the EDCs. Δ_{band} ~ 10 meV is extracted from the fitted dispersions, which is smaller than that in the pure LiFeAs compound.

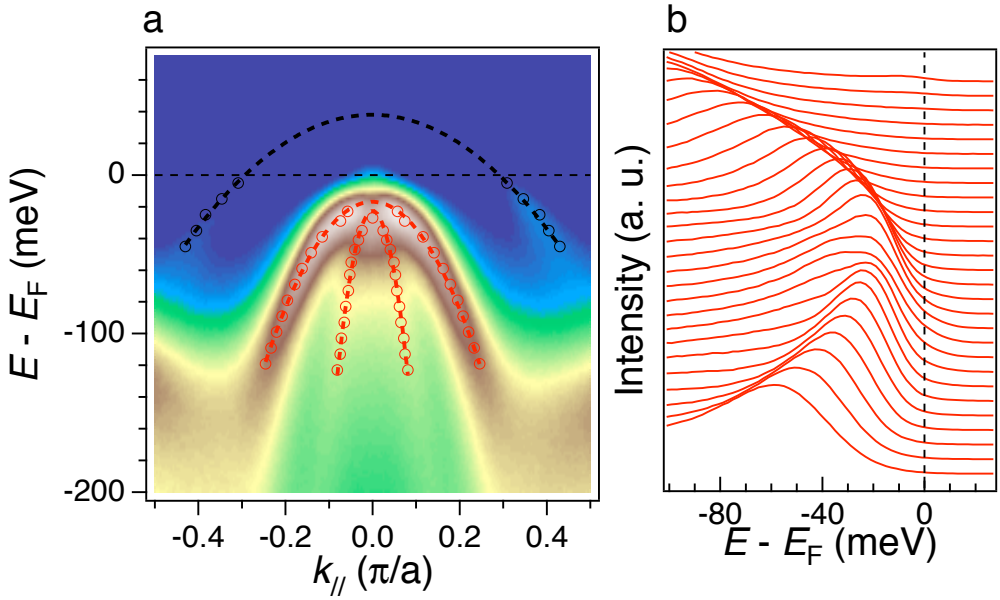

S4: ARPES data of $LiFe_{0.94}Co_{0.06}As$

2.4 Extraction of Δ_{band}

To precisely evaluate Δ_{band} as function of temperature, the extracted band dispersions, EDCs and MDCs are used in our study and all those methods show that the d_{xz}/d_{yz} splitting is decreased from 14 meV at 50 K to nearly 0 at 250 K.

A. Band dispersion:

The band dispersions of the α, α' and β bands at different temperatures are carefully extracted from EDCs and MDCs and fitted to the parabolic function:

$$E(k) = a(T) + b(T) \times k^2 \qquad (5)$$

Since only the α band exhibits visible change from low temperature to high temperature, we only show its fitted parameters in table 1.

Table 1

	50 K	100 K	150 K	200 K	250 K
a (meV)	2	2	0.7	-5	-10
b (meV•Å^{-2})	1200	1000	990	930	920
Δ_{band} (meV)	14 ± 1	14 ± 1	13 ± 3	7 ± 4	2 ± 4

From the fitted the data, we find that the α band is shifted down by about 12 meV as temperature is increased from 50 K to 250 K. Since the α' and β bands are barely changed from low temperature to high temperature, the observed shift of the α band is exactly the change of Δ_{band}.

B. Momentum distribution Curves (MDCs)

Δ_{band} can also be evaluated by using MDCs. Fig. 3l of the main text shows temperature dependent MDCs at 20 meV below E_F. We find that only the peak position of the α band becomes closer as temperature increases, proving that the α band is shifted downward at high temperature, which is consistent with the extracted band dispersions. To quantitatively evaluate Δ_{band} from the MDCs, we rewrite Eq (5), and get:

$$\Delta_{band} \approx 2b_{ave} \times k_{ave} \times \Delta k \qquad (6)$$

Here we use four-Lorentz peaks to fit MDCs and get the result below:

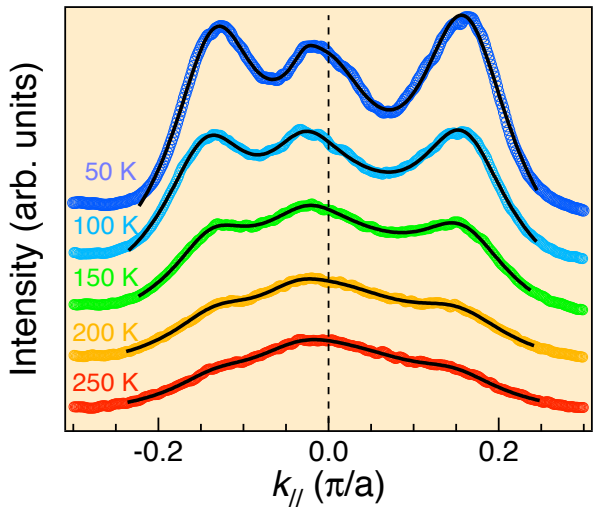

S5 : Fitted MDCs

The fitted peak positions of the α' band at 20 meV below E_F are :

Table 2

	50 K	100 K	150 K	200 K	250 K
Peak (π/a)	0.176	0.175	0.173	0.160	0.145

The extracted band splitting obtained by all methods are plotted in Fig. 3m and shows a consistent trend at high temperature.

C. Energy Distribution Curves (EDCs)

Another way to evaluate Δ_{band} is by directly fitting EDCs across the Γ point by using two Lorentzian peaks.

$$I[\vec{k} = (0,0),\omega] = c_0 + \frac{a_1\Gamma_1}{((\omega - x_1)^2 + \Gamma_1^2)} + \frac{a_2\Gamma_2}{((\omega - x_2)^2 + \Gamma_2^2)} \quad (7)$$

The matrix element effect is included in the fitting parameters $a_{1,2}$, and we further assume that Γ(k, ω) is independent of ω near E_F.

The fitted results are shown in Fig. S6 and Table 3, as well as in Fig. 3k of the main text. Below 150 K, the band top of the α and α' bands are clearly separated in the raw data and can be well fitted by two Lorentzian peaks. The fitted result shows that the α' band remains unchanged below 150 K while the α band starts to shift downward at 150 K, which is consistent with

the results extracted from the band dispersion and from the MDCs. Above 150 K, due to lifetime broadening and to the closeness of the α and α' bands, two peak structures are merged together and only the main peak position can be extracted by using a single Lorentzian function. As shown in Fig. S6, EDCs at 200 K and 250 K are nicely fitted by a single Lorentzian function with peak positions at 9 meV and 11 meV below E_F. The shift of the main peak position proves that the α band keeps moving downward above 150 K and eventually becomes degenerate with the top of the α' band at 250 K. These results are again consistent with the previous ones extracted for the temperature evolution of Δ_{band}.

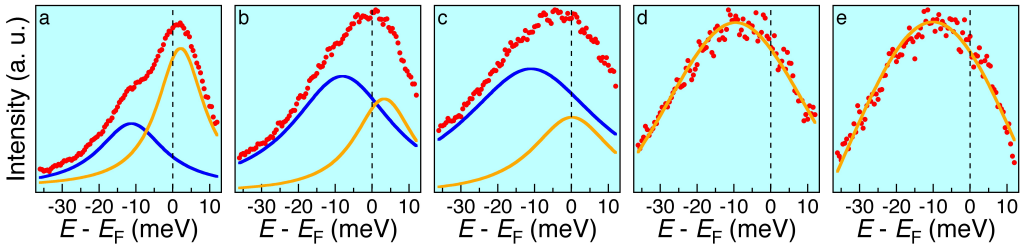

S6: Fitted EDCs

Table 3

	50 K	100 K	150 K	200 K*	250 K*
x_1 (meV)	2 ± 0.5	3 ± 1	0 ± 1	-9 ± 1	-11 ± 1
Γ_1 (meV)	11 ± 0.5	17 ± 2	23 ± 5	33 ± 3	41 ± 7
x_2 (meV)	-11.5 ± 0.5	-10 ± 1	-11 ± 2	–	–
Γ_1 (meV)	8 ± 0.5	10 ± 1	15 ± 3	–	–
Δ (meV)	13.5 ± 1	13 ± 2	11 ± 2	3 ± 3*	2 ± 3*

*: When extracting Δ_{band} at 200 K and 250 K, we used the main peak position to represent the peak position of the α band. This will slightly underestimate the value of Δ_{band}.

2.5 d_{xz}/d_{yz} splitting near the M point:

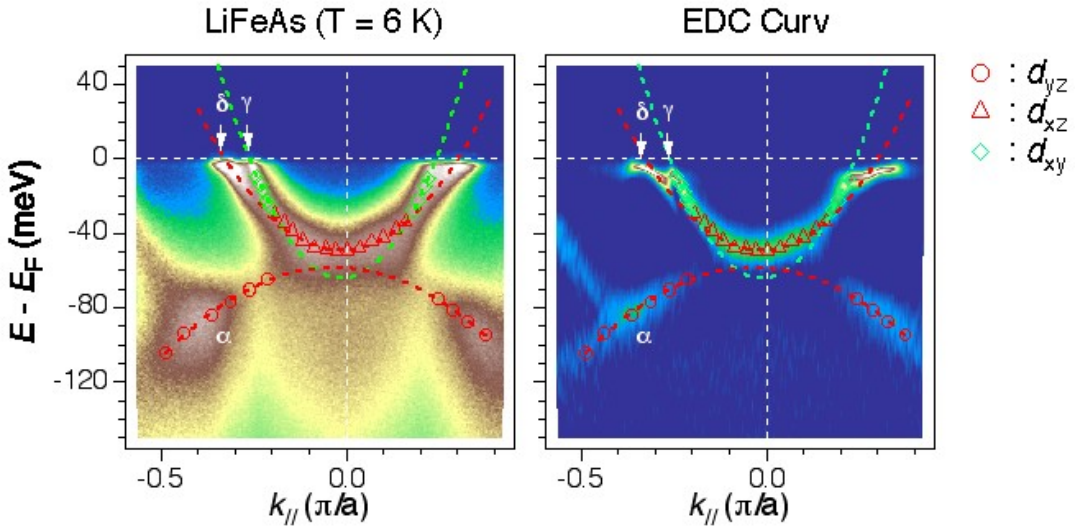

S7 ARPES intensity and EDC curvature plot at the M point

Fig. S7 shows ARPES intensity and EDC curvature plots. Two electron pockets, δ and γ, which have d_{xz}/d_{yz} and d_{xy} orbitals respectively, are clearly

resolved. Below the two electron pockets, the α band with d_{xz}/d_{yz} orbitals is dispersed from the Γ point to the M point and expected to be degenerate with the δ band if no nematic fluctuation is present. By using the EDC curvature plot, we precisely extracted the band dispersions of the α, δ and γ bands, and fitted them using parabolic functions. It is clear from the plot that the α and δ bands are split with a band gap of $\Delta_M = 8 \pm 2$ meV, which is about the half the value of $\Delta_\Gamma = 14$ meV.

The observed degeneracy lifting at the M point rules out the SOC as the origin of the observed d_{xz}/d_{yz} splitting at the Γ point. Furthermore, the smaller splitting value at the M point indicates that the spin nematic fluctuations might be small, which is consistent with NMR results in LiFeAs.

2.6 Two branch dispersion on the δ band:

Since the ferro-orbital correlations break the local tetragonal symmetry, it is expected to observe a two-branch dispersions on the d_{xz}/d_{yz} bands. As shown in Fig. 1 of the main text, the two-branch behavior is clearly resolved near the Γ point. Here we show the high resolution data on the δ band, which also has d_{xz}/d_{yz} orbitals.

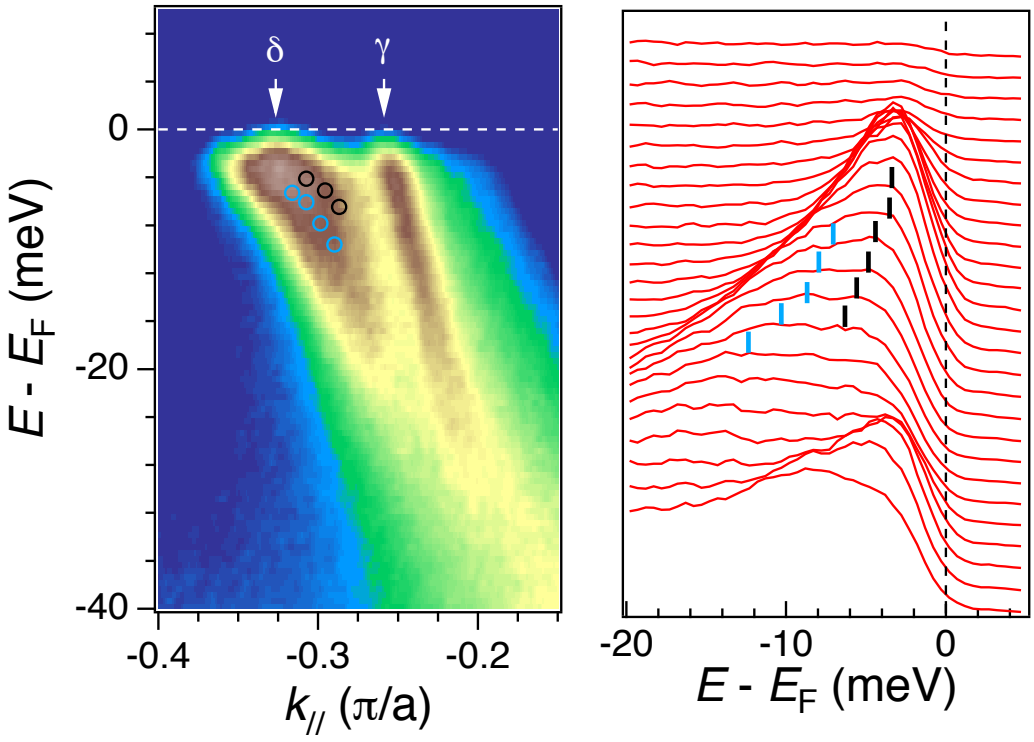

S8: Intensity plot and EDCs of δ band near E_F

As shown in Fig. S8a, we find that the δ band is broader near E_F, which clearly deviates from the Landau's quasi-particle picture. By analyzing the corresponding EDCs, as shown in Fig. S8b, we find that as with the α band, the δ band also has two branches. The observed twined structure near both the Γ and the M points is strongly against the SOC scenario and supports the ferro-orbital fluctuations picture.

3. Theoretical demonstration of degeneracy lifting under long-range correlations in the absence of an order

To demonstrate the effects of long-range ferro-orbital (FO) correlations without ordering, let's first consider a 2D two-band system under the influence of a diagonal local FO order parameter τ_i:

$$H = \sum_{ij} t_{ij}\left(c_i^+ c_j + d_i^+ d_j\right) + \sum_i \tau_i\left(c_i^+ c_i - d_i^+ d_i\right)$$

where c^+ and d^+ correspond to creation of particles in each band, and t_{ij} is a strongly anisotropic quasi-1D hopping parameter with value 1 in one direction and 0.01 in the other. The diagonal local parameter is Ising-like and either takes the values 1 or -1.

For a simple demonstration, here the coupling between c^+ and d^+ is assumed negligible to keep these two bands fully degenerate in the entire momentum-space. Consequently, the problem can be decoupled into two equivalent single-band ones:

$$H = \sum_{ij} t_{ij} c_i^+ c_j + \sum_i \tau_i c_i^+ c_i$$
$$H = \sum_{ij} t_{ij} d_i^+ d_j - \sum_i \tau_i d_i^+ d_i$$

We then numerically measure the one-particle Green's function[4], while sampling[5] the Ising configuration space of τ_i, using the Monte Carlo method[6] with the Metropolis algorithm.

The key technical issue here is how to prepare the configuration space and its corresponding probability, to survey both short-range and long-range correlations in the absence of an order. Intuitively, the most natural choice is to use the 2D Ising model and tune the temperature. However, in that case the long-range power-law decay of the correlations only occurs very close to the critical temperature, where numerical studies suffer from critical slow down. Instead, we have generated the configurations and their probabilities using the 2D *xy*-model, and defined the FO order parameter from the sign of the *x*-component of the local *xy*-spin $S_{\mathrm{i}}^{\mathrm{x}}$:

$$\tau_i = sign(S_i^x)$$

This way, there is a large temperature range away from the critical temperature where a power-law decay correlation function of τ can be found. For a simple and representative example of exponential-decaying short-range correlations, the temperature is chosen to be infinity.

Our results are found to converge very well at size 32x32 sites. In fact, the size of the splitting remains almost size independent, but only the smoothness of the resulting spectral function and the location of resonances show some size dependence.

References:

1. X.-P. Wang, P. Richard, Y.-B. Huang, H. Miao, L. Cevey, N. Xu, Y.-J. Sun, T. Qian, Y.-M. Xu, M. Shi, J.-P. Hu, X. Dai and H. Ding, Orbital characters determined from Fermi surface intensity patters using angle-resolved photoemission spectroscopy. *Phys. Rev. B* **85**, 214518 (2012).

2. Y.-M. Xu, Y.-B. Huang, X.-Y. Cui, E. Razzoli, M. Radovic, M. Shi, G.-F. Chen, P. Zheng, N.-L.Wang, C.-L. Zhang, P.-C. Dai, J.-P. Hu, Z. Wang and H. Ding, Observation of a ubiquitous three dimensional superconducting gap function in optimally doped $Ba_{0.6}K_{0.4}Fe_2As_2$. *Nature Phys*, **7**, 198 (2011).

3. Z. R. Ye, Y. Zhang, M. Xu, Q. Q. Ge, Q. Fan, F. Chen, J. Jiang, P. S. Wang, J. Dai, W. Yu, B. P. Xie, D. L. Feng, Orbital selective correlations between nesting/scattering/Lifshitz transition and the superconductivity in $AFe_{1-x}Co_xAs$ (A= Li, Na). Preprint at http://arxiv.org/abs/1303.0682 (2013).

4. W. Ku T. Berlijn and C.-C. Lee, Unfolding First-Principles Band Structures . *Phys. Rev. Lett.* **104**, 216401 (2010).

5. **T.** Berlijn, V. Dmitri and W. Ku. Can Disorder Alone Destroy the e_g' Hole Pockets of Na_xCoO_2? A Wannier Function Based First-Principles Method for Disordered Systems. *Phys. Rev. Lett.* **106**, 077005 (2011).

6. David Chandler, Introduction of Modern Statistical Mechanism, Oxford (1987).